The effect of stratification on the wave number selection in the instability of sedimenting spheroids

David Saintillan[a)]
Department of Mechanical Engineering, Stanford University, Stanford, California 94305

Eric S. G. Shaqfeh
Department of Chemical Engineering, Department of Mechanical Engineering, and Institute for Computational and Mathematical Engineering, Stanford University, Stanford, California 94305

Eric Darve
Department of Mechanical Engineering and Institute for Computational and Mathematical Engineering, Stanford University, Stanford, California 94305

(Received 3 April 2006; accepted 28 July 2006; published online 8 December 2006)

It is well known that a dilute suspension of spheroids sedimenting under gravity at low Reynolds number is unstable to density fluctuations as a result of hydrodynamic interactions [D. L. Koch and E. S. G. Shaqfeh, J. Fluid Mech. **209**, 521 (1989)]. Using a linear stability analysis, it is shown that a vertical density gradient in such a suspension can lead to a wave number selection by damping fluctuations at long wavelengths. A scaling for the most unstable wavelength, or characteristic size of the density fluctuations, is obtained in terms of the background stratification and volume fraction, and is compared to results from numerical simulations in stratified particulate suspensions using methods that we have developed previously. In initially homogeneous suspensions, simulations show a continuous decay of the size of the density fluctuations over time, which we demonstrate can be attributed to the development of stratification inside the suspension. © *2006 American Institute of Physics*. [DOI: 10.1063/1.2396913]

I. INTRODUCTION

The long-ranged nature of hydrodynamic interactions in the low-Reynolds-number sedimentation of a dilute suspension results in strong velocity fluctuations.[1–5] These fluctuations are driven by the random arrangement of the particles in the suspension, and have typical magnitudes that can exceed the mean settling rate. When the suspended particles are nonspherical, the coupling between the disturbance flow in the fluid and the particle orientations also results in a concentration instability, by which an initially well-mixed suspension develops inhomogeneities. This instability was first predicted theoretically in the case of rigid spheroids by Koch and Shaqfeh,[6] who observed that the disturbance flow induced by the random density fluctuations causes the particles to orient in such a way that they migrate toward the regions of higher particle density. Koch and Shaqfeh also performed a linear stability analysis in an unbounded homogeneous suspension, and showed that low-wave-number fluctuations should indeed amplify, with a maximum growth rate for a horizontal wave with zero wave number. Based on their analysis, the characteristic size of the density fluctuations in a bounded system should therefore scale with the container dimensions.

The instability was subsequently observed both in experiments[7–9] and numerical simulations.[10–15] Simulations of periodic suspensions[10,11,13,15] qualitatively agree with the analysis described above, and show the formation of a single dense streamer surrounded by clarified fluid, confirming that the longest wavelength is the most unstable in such systems. However, experiments by Guazzelli and co-workers report the formation of clusters that are typically smaller than the container dimensions, with sizes of the order of a few particle lengths.[7,8] Recently, Metzger, Guazzelli, and Butler[9] studied the evolution of the microstructure in dilute fiber suspensions under sedimentation, and observed that the sedimentation process is initially characterized by the formation of one large-scale streamer spanning half of the container width, followed by a transition to multiple streamers and backflow regions alternating in the horizontal direction. While the initial growth of a single streamer agrees qualitatively with the theoretical prediction,[6] the subsequent wave number selection is not accounted for by the stability analysis, and must therefore involve mechanisms heretofore not included in the stability theory, such as interactions with the container boundaries or stratification.

In our recent work,[14] we confirmed the importance of container walls in the wave number selection of the instability. Using a point-particle method, we performed numerical simulations of large-scale suspensions in finite containers, in which a tangential flow boundary condition was enforced on the walls. Unlike the simulations in periodic systems, these simulations in finite containers did capture a transition from a single box-dependent streamer to multiple structures at shorter wavelengths, in good qualitative agreement with the experimental observations.[9] The wavelength of the instability

[a)]Present address: Courant Institute of Mathematical Sciences, New York University, New York, NY 10012.

seemed to reach a steady value in the simulations; yet this value was typically reached shortly before the approach of the sedimentation front, so that it is not entirely clear whether a true steady state would be observed in larger suspensions. The precise mechanism leading to the decay of the size of the fluctuations over time was not elucidated. We speculated that the recirculation currents taking place as a result of the horizontal container boundaries may homogenize the suspension over large length scales, leading to the suppression of the fluctuations below a finite wave number. It was also suggested that the strong stratification that was shown to develop in the suspensions may have an effect on the instability by damping the velocity fluctuations.

The effects of stratification on the velocity fluctuations in suspensions of sedimenting spheres have been considered in a few studies.[4,5,16,17] Luke[16] first suggested that a stable vertical density gradient should lead to a decay of the velocity fluctuations over time: the physical argument that he proposed is that density fluctuations settle rapidly toward their equilibrium position, after which they no longer contribute to the variance of the velocity. According to Luke,[16] this mechanism should result in a decay of the velocity variance as $t^{-1/2}$, precluding the existence of a steady state. This original idea was then re-examined by Brenner and co-workers,[5,17] who argued that density fluctuations in a suspension are simultaneously damped by stratification and generated by random fluctuations in the particle motions; by balancing the effects of stratification and hydrodynamic dispersion, they were therefore able to derive a scaling for the velocity fluctuations, in good accord with results from their experiments and numerical simulations. Although there appears to be a consensus on the damping effect of a stable vertical density gradient on the fluctuations, the presence and the origin of stratification in sphere suspensions are still debated.[4,18]

In the case of anisotropic particles such as spheroids, the dispersion in orientation, which causes particles with different orientations to settle at different speeds, and the concentration fluctuations, which result in the fast settling of the dense clusters with respect to the clarified regions, both lead to a strong stratification.[9,14,19] In this paper we address the effect of this stratification on the fluctuations in suspensions of spheroids. More specifically, we examine the relationship between stratification and the concentration instability described above,[6] with the aim of elucidating the wave number selection process observed experimentally[9] and in simulations.[14] The paper is organized as follows: in Sec. II we revisit the linear stability analysis of Koch and Shaqfeh[6] in the case of a stably stratified suspension, where we also account for center-of-mass hydrodynamic dispersion. We show that stratification can provide a mechanism for wave number selection, and a scaling for the most unstable mode is derived in Sec. III. We then test this scaling in Sec. IV against results from large-scale numerical simulations of both stratified and initially well-mixed suspensions. A summary and concluding remarks are given in Sec. V.

II. LINEAR STABILITY ANALYSIS

A. Governing equations

Following Koch and Shaqfeh,[6] we describe a dilute suspension of spheroids using a continuous variable $c(\boldsymbol{x},\boldsymbol{p})$ denoting the concentration of particles at location $\boldsymbol{x}$ with orientation $\boldsymbol{p}$, where $\boldsymbol{p}$ is a unit vector aligned with the major axis of a given spheroid. Particle conservation requires the following convective-diffusion equation to apply:

$$\frac{\partial c}{\partial t} + \nabla_p \cdot (\dot{\boldsymbol{p}} c) + \nabla_x \cdot (\dot{\boldsymbol{x}} c) - \nabla_x \cdot (\mathbf{D} \cdot \nabla_x c) = 0. \tag{1}$$

In addition to the convective terms previously considered by Koch and Shaqfeh, we also account for center-of-mass hydrodynamic dispersion through the diffusion tensor $\mathbf{D}$. We shall assume that the diffusion tensor does not depend on the particle orientations, but takes on the following anisotropic form: $\mathbf{D}=D_{\parallel}\hat{z}\hat{z}+D_{\perp}(\mathbf{I}-\hat{z}\hat{z})$, where $\hat{z}$ is a unit vector in the vertical direction. Note that in a real system, rotational dispersion is also expected to occur: for simplicity this effect will be neglected here.

The convective fluxes in Eq. (1) involve the linear and angular velocities of a particle. In the dilute limit, the linear velocity $\dot{\boldsymbol{x}}$ is obtained as the sum of the sedimentation velocity in orientation $\boldsymbol{p}$ and of the bulk disturbance velocity at position $\boldsymbol{x}$:

$$\dot{\boldsymbol{x}} = \boldsymbol{U}_s(\boldsymbol{p}) + \boldsymbol{u}(\boldsymbol{x}). \tag{2}$$

For a spheroidal particle, the sedimentation velocity is obtained as

$$\boldsymbol{U}_s(\boldsymbol{p}) = (\lambda_0 \mathbf{I} + \lambda_1 \boldsymbol{pp}) \cdot \boldsymbol{F}, \tag{3}$$

where λ_0 and λ_1 are known functions of the length l and aspect ratio A of the spheroid, and of the viscosity μ of the suspending fluid.[20] In Eq. (3), $\boldsymbol{F}$ denotes the gravity force acting on a particle $\boldsymbol{F}=-F\hat{z}=-\Delta\rho V_p g\hat{z}$, where $\Delta\rho$ is the density difference between the solid and fluid phases, V_p is the volume of the particle, and g is the acceleration of gravity. The disturbance fluid velocity $\boldsymbol{u}$ appearing in Eq. (2) is driven by the density fluctuations in the suspension, and to leading order satisfies the Stokes equations including a body force proportional to the local concentration:

$$-\mu\nabla^2\boldsymbol{u} + \nabla p = \boldsymbol{F}\int c(\boldsymbol{x},\boldsymbol{p})d\boldsymbol{p}, \quad \nabla\cdot\boldsymbol{u}=0. \tag{4}$$

Finally, the angular velocity $\dot{\boldsymbol{p}}$ of a spheroid is induced by the local disturbance flow in the fluid, and in the dilute limit is captured using Jeffery's equation:[21]

$$\dot{\boldsymbol{p}} = (\mathbf{I}-\boldsymbol{pp})\cdot[\gamma\mathbf{E}(\boldsymbol{x}) + \boldsymbol{\Omega}(\boldsymbol{x})]\cdot\boldsymbol{p}, \tag{5}$$

where $\mathbf{E}(\boldsymbol{x})=[\nabla\boldsymbol{u}(\boldsymbol{x})+\nabla\boldsymbol{u}(\boldsymbol{x})^T]/2$ and $\boldsymbol{\Omega}(\boldsymbol{x})=[\nabla\boldsymbol{u}(\boldsymbol{x}) - \nabla\boldsymbol{u}(\boldsymbol{x})^T]/2$ denote the local disturbance rate of strain and rate of rotation tensors, respectively, and where γ stands for Jeffery's parameter: $\gamma\equiv(A^2-1)/(A^2+1)$.

The dynamic equations (2) and (5) are exact if the local velocity field is linear on the scale of the particle; in a nonlinear flow additional corrections involving higher-order velocity gradients would have to be included. The present de-

scription is therefore only valid in dilute suspensions, in which the characteristic distance between particles is much greater than their size $nl^3 \ll 1$, where n denotes the mean number density. Similarly, Eq. (4) assumes that the only effect of a given particle on the fluid flow is given by a point force; this approximation, which corresponds to the leading-order term in a multipole expansion of the disturbance velocity induced by a sedimenting particle, is also limited to dilute suspensions.

B. Base state and linearized equations

To extend the results of Koch and Shaqfeh,[6] who only considered density fluctuations with respect to a uniform distribution of isotropically oriented particles, we now allow for a vertical density gradient in the background concentration. More precisely, we assume that the density field in the base state is linearly stratified. At $t=0$

$$c(\boldsymbol{x},\boldsymbol{p},0) = n\Psi(\boldsymbol{p})(1-\beta z). \tag{6}$$

In particular, we also allow for an anisotropic orientation distribution $\Psi(\boldsymbol{p})$ in the base state; the isotropic case is easily recovered by setting $\Psi(\boldsymbol{p})=(4\pi)^{-1}$. In the following discussion we shall only consider stably stratified suspensions, for which $\beta \geq 0$. Substitution of Eq. (6) into the Stokes equations (4) shows that the density gradient is balanced by a pressure gradient $\nabla p = -Fn(1-\beta z)\hat{z}$, and does not induce a mean flow. Therefore in the base state the velocity and pressure fields in the suspension are given by $\boldsymbol{u}(\boldsymbol{x})=\boldsymbol{0}$, and $p(\boldsymbol{x})=p_0-F(z-\beta z^2/2)$. The stratified density field is advected downwards as follows:

$$c(\boldsymbol{x},\boldsymbol{p},t) = n\Psi(\boldsymbol{p})[1-\beta(z-\hat{z}\cdot\boldsymbol{U}_s(\boldsymbol{p})t)], \tag{7}$$

which is an exact solution of the conservation equation (1). Note in particular that because particles with different orientations sediment at different speeds, the orientation distribution at a given vertical station will evolve in time.

To investigate the stability of the suspension, we consider a weak perturbation with respect to the base state:

$$c(\boldsymbol{x},\boldsymbol{p},t) = n\Psi(\boldsymbol{p})[1-\beta(z-\hat{z}\cdot\boldsymbol{U}_s(\boldsymbol{p})t)] + \varepsilon c'(\boldsymbol{x},\boldsymbol{p},t), \tag{8}$$

where $|\varepsilon| \ll 1$ and $|c'(\boldsymbol{x},\boldsymbol{p},t)| \sim O(n/4\pi)$. This perturbation induces a weak disturbance flow: $\boldsymbol{u}(\boldsymbol{x})=\varepsilon\boldsymbol{u}'(\boldsymbol{x})$ (with an associated pressure perturbation $p=\varepsilon p'$), which in turn causes the rotation of the particles at the angular velocity $\dot{\boldsymbol{p}}=\varepsilon\dot{\boldsymbol{p}}'$. Substituting the perturbed density field equation (8) into the conservation equation (1), and identifying terms of order ε yields the following linearized equation for the density fluctuations:

$$\frac{\partial c'}{\partial t} + n\Psi(\boldsymbol{p})[1-\beta(z-\hat{z}\cdot\boldsymbol{U}_s(\boldsymbol{p})t)]\nabla_p\cdot\dot{\boldsymbol{p}}' + n\dot{\boldsymbol{p}}'\cdot\nabla_p\{\Psi(\boldsymbol{p})[1-\beta(z-\hat{z}\cdot\boldsymbol{U}_s(\boldsymbol{p})t)]\} + \boldsymbol{U}_s\cdot\nabla_x c' - \beta n\Psi(\boldsymbol{p})\hat{z}\cdot\boldsymbol{u}' - \nabla_x\cdot(\mathbf{D}\cdot\nabla_x c') = 0, \tag{9}$$

where we made use of the incompressibility condition $\nabla\cdot\boldsymbol{u}'=0$. In Eq. (9) the disturbance velocity field $\boldsymbol{u}'$ and angular velocity $\dot{\boldsymbol{p}}'$ still satisfy Eqs. (4) and (5), respectively, with primed variables. Note in particular that the coefficients in Eq. (9) are time-dependent, which is a consequence of having a time-dependent base state [Eq. (7)]. In general such a stability problem could be solved using Floquet theory.[23] Here we limit ourselves to the case of short times and weak density gradients, i.e., we restrict our analysis to length and time scales that satisfy the following condition: $|z-\hat{z}\cdot\boldsymbol{U}_s(\boldsymbol{p})t| \ll \beta^{-1}$. In particular, the characteristic wavelength of the instability should remain smaller than the stratification length scale β^{-1}, and our results will only be valid over time scales shorter than the characteristic time $(\beta\lambda_0 F)^{-1}$ for a particle to sediment over the stratification length β^{-1}. As we shall see in the numerical simulations of Sec. IV, the stratification length β^{-1} in the bulk of the suspensions typically remains of the order of the height of the simulation box or larger (except near the very end of the simulations), in which case both conditions are indeed satisfied. Under these assumptions, the linearized conservation equation is simplified as follows:

$$\frac{\partial c'}{\partial t} + n\Psi(\boldsymbol{p})\nabla_p\cdot\dot{\boldsymbol{p}}' + n\dot{\boldsymbol{p}}'\cdot\nabla_p\Psi(\boldsymbol{p}) + \boldsymbol{U}_s\cdot\nabla_x c' - \beta n\Psi(\boldsymbol{p})\hat{z}\cdot\boldsymbol{u}' - \nabla_x\cdot(\mathbf{D}\cdot\nabla_x c') = 0. \tag{10}$$

C. Dispersion relation

To achieve analytical progress, we consider the evolution of a density perturbation written as a plane wave of wave vector $\boldsymbol{k}$ and complex frequency $\omega \equiv \omega_R + i\omega_I$:

$$c'(\boldsymbol{x},\boldsymbol{p}) = \tilde{c}(\boldsymbol{k},\boldsymbol{p},\omega)\exp i(\boldsymbol{k}\cdot\boldsymbol{x}-\omega t). \tag{11}$$

We wish to determine the dispersion relation $\omega(\boldsymbol{k})$ allowing for such modes to satisfy the linearized conservation equation (10), and more specifically to identify the wave vectors $\boldsymbol{k}$ leading to positive growth rates, i.e., positive values of the imaginary part ω_I of the frequency.

By linearity of the Stokes equation (4), the disturbance velocity induced by the density perturbation equation (11) can also be written as a plane wave of the same wave vector and frequency: $\boldsymbol{u}'(\boldsymbol{x})=\tilde{\boldsymbol{u}}(\boldsymbol{k},\omega)\exp i(\boldsymbol{k}\cdot\boldsymbol{x}-\omega t)$, where the Fourier coefficient $\tilde{\boldsymbol{u}}(\boldsymbol{k},\omega)$ is obtained analytically as[22]

$$\tilde{\boldsymbol{u}}(\boldsymbol{k},\omega) = \frac{1}{\mu k^2}(\mathbf{I}-\hat{\boldsymbol{k}}\hat{\boldsymbol{k}})\cdot\boldsymbol{F}\int\tilde{c}(\boldsymbol{k},\boldsymbol{p},\omega)d\boldsymbol{p}, \tag{12}$$

where we use the notation $\hat{\boldsymbol{k}} \equiv \boldsymbol{k}/|\boldsymbol{k}|$. Substituting this expression into Jeffery's Eq. (5) allows us to calculate the Fourier coefficient $\dot{\tilde{\boldsymbol{p}}}(\boldsymbol{k},\boldsymbol{p},\omega)$ of the angular velocity, as well as its orientational divergence:

$$\dot{\tilde{\boldsymbol{p}}}(\boldsymbol{k},\boldsymbol{p},\omega) = \frac{i}{2\mu k^2}(\mathbf{I}-\boldsymbol{pp})\cdot[(\gamma+1)(\boldsymbol{p}\cdot\boldsymbol{k})\mathbf{I} + (\gamma-1)\boldsymbol{kp}]\cdot(\mathbf{I}-\hat{\boldsymbol{k}}\hat{\boldsymbol{k}})\cdot\boldsymbol{F}\int\tilde{c}d\boldsymbol{p}, \tag{13}$$

$$\nabla_p\cdot\dot{\tilde{\boldsymbol{p}}}(\boldsymbol{k},\boldsymbol{p},\omega) = -\frac{3i\gamma}{\mu k^2}(\boldsymbol{p}\cdot\boldsymbol{k})\boldsymbol{p}\cdot(\mathbf{I}-\hat{\boldsymbol{k}}\hat{\boldsymbol{k}})\cdot\boldsymbol{F}\int\tilde{c}d\boldsymbol{p}. \tag{14}$$

Using Eqs. (11)–(14) for the Fourier coefficients of the concentration fluctuations, disturbance velocity, and angular ve-

locity, we find that the linearized conservation equation (10) becomes

$$(i\boldsymbol{k}\cdot\boldsymbol{U}_s - i\omega + \boldsymbol{k}\cdot\mathbf{D}\cdot\boldsymbol{k})\tilde{c} - \frac{n\Psi(\boldsymbol{p})}{\mu k^2}[\beta\hat{\boldsymbol{z}} + 3i\gamma(\boldsymbol{p}\cdot\boldsymbol{k})\boldsymbol{p}]$$
$$\cdot(\mathbf{I}-\hat{\boldsymbol{k}}\hat{\boldsymbol{k}})\cdot\boldsymbol{F}\int\tilde{c}d\boldsymbol{p} + \frac{in}{2\mu k^2}\nabla_p\Psi(\boldsymbol{p})\cdot(\mathbf{I}-\boldsymbol{pp})$$
$$\cdot[(\gamma+1)(\boldsymbol{p}\cdot\boldsymbol{k})\mathbf{I} + (\gamma-1)\boldsymbol{kp}]\cdot(\mathbf{I}-\hat{\boldsymbol{k}}\hat{\boldsymbol{k}})\cdot\boldsymbol{F}\int\tilde{c}d\boldsymbol{p} = 0. \tag{15}$$

Following Koch and Shaqfeh,[6] we divide Eq. (15) by $(i\boldsymbol{k}\cdot\boldsymbol{U}_s - i\omega + \boldsymbol{k}\cdot\mathbf{D}\cdot\boldsymbol{k})$ and integrate over orientation space. We also introduce the following dimensionless variables:

$$\boldsymbol{k}^* = \boldsymbol{k}\left(\frac{\mu\lambda_1}{n}\right)^{1/2},\quad \omega^* = \omega\left(\frac{\mu}{n\lambda_1 F^2}\right)^{1/2},\quad \lambda = \frac{\lambda_0}{\lambda_1},$$
$$\beta^* = \beta\left(\frac{\mu\lambda_1}{n}\right)^{1/2},\quad \mathbf{D}^* = \mathbf{D}\left(\frac{n}{\mu\lambda_1^3 F^2}\right)^{1/2}. \tag{16}$$

After simplifications, we arrive at the following dimensionless dispersion relation, which is an equation for $\omega^*(\boldsymbol{k}^*)$:

$$1 + \frac{1}{k^{*2}}\int\Psi(\boldsymbol{p})\left[\frac{\beta^*\hat{\boldsymbol{z}} + 3i\gamma(\boldsymbol{p}\cdot\boldsymbol{k}^*)\boldsymbol{p}}{i\boldsymbol{k}^*\cdot\boldsymbol{U}_s^* - i\omega^* + \boldsymbol{k}^*\cdot\mathbf{D}^*\cdot\boldsymbol{k}^*}\right]$$
$$\cdot(\mathbf{I}-\hat{\boldsymbol{k}}\hat{\boldsymbol{k}})\cdot\hat{\boldsymbol{z}}d\boldsymbol{p} - \frac{i}{2k^{*2}}\int\nabla_p\Psi(\boldsymbol{p})$$
$$\cdot(\mathbf{I}-\boldsymbol{pp})\cdot\left[\frac{(\gamma+1)(\boldsymbol{p}\cdot\boldsymbol{k}^*)\mathbf{I} + (\gamma-1)\boldsymbol{k}^*\boldsymbol{p}}{i\boldsymbol{k}^*\cdot\boldsymbol{U}_s^* - i\omega^* + \boldsymbol{k}^*\cdot\mathbf{D}^*\cdot\boldsymbol{k}^*}\right]$$
$$\cdot(\mathbf{I}-\hat{\boldsymbol{k}}\hat{\boldsymbol{k}})\cdot\hat{\boldsymbol{z}}d\boldsymbol{p} = 0, \tag{17}$$

where the dimensionless sedimentation velocity is given by $\boldsymbol{U}_s^*(\boldsymbol{p}) = -(\lambda\mathbf{I}+\boldsymbol{pp})\cdot\hat{\boldsymbol{z}}$. The original dispersion relation of Koch and Shaqfeh[6] can be recovered by neglecting stratification and center-of-mass dispersion ($\beta^*=0$ and $\mathbf{D}^*=\mathbf{0}$), and by considering the case of an isotropic orientation distribution: $\Psi(\boldsymbol{p}) = (4\pi)^{-1}$.

A general solution of Eq. (17) is not easily obtained. In the present work we limit our discussion to the case of horizontal waves, for which $\boldsymbol{k}\cdot\hat{\boldsymbol{z}}=0$. These waves are indeed known to be the most unstable in the isotropic homogeneous case.[6] We first investigate the case of isotropic suspensions in Sec. II D, for which the dispersion relation greatly simplifies, and then discuss the effect of an anisotropic orientation distribution in Sec. II E.

D. Isotropic case

In the case of a horizontal wave with an isotropic orientation distribution, the dispersion relation (17) is simplified as follows:

$$1 + \frac{1}{4\pi k^{*2}}\int\left[\frac{i\beta^* - 3\gamma(\boldsymbol{p}\cdot\boldsymbol{k}^*)(\boldsymbol{p}\cdot\hat{\boldsymbol{z}})}{(\boldsymbol{p}\cdot\boldsymbol{k}^*)(\boldsymbol{p}\cdot\hat{\boldsymbol{z}}) + \omega^* + ik^{*2}D_\perp^*}\right]d\boldsymbol{p} = 0. \tag{18}$$

We expect the complex frequency ω^* to be pure imaginary: solutions with $\omega_R^*>0$ would indeed correspond to traveling or standing waves in the direction of $\boldsymbol{k}^*$, which are not physical when $\boldsymbol{k}^*$ points in the horizontal direction. We therefore look for solutions written as $\omega^* = i\omega_I^*$, and solve Eq. (18) numerically using quadrature and a bisection algorithm. Figure 1 shows the calculated normalized growth rate (or imaginary part ω_I^* of the complex frequency) for the most unstable modes at the given value of $D_\perp^*=0.02$ and for various values of β^*. In the absence of stratification ($\beta^*=0$), the growth rate is found to be the greatest at zero wave number. This is analogous to the result of Koch and Shaqfeh,[6] with the difference that center-of-mass dispersion now causes a more rapid decay of the growth rate at high wave numbers. This stabilizing effect of center-of-mass dispersion is similar to that observed previously in the case of sedimenting deformable particles.[14] Adding stratification ($\beta^*>0$) however results in a qualitatively different picture. The shortest wave numbers ($k^*\gtrsim 0$) are stabilized, and a maximum growth rate is observed at a finite positive wave number. As stratification becomes stronger, i.e., as β^* increases, the most unstable wave number increases while the maximum growth rate decreases. Beyond a certain level of stratification the instability is suppressed. As seen in Fig. 1, some values of k^* yield two pure imaginary roots for ω^*, in which case the largest growth rate is expected to dominate.

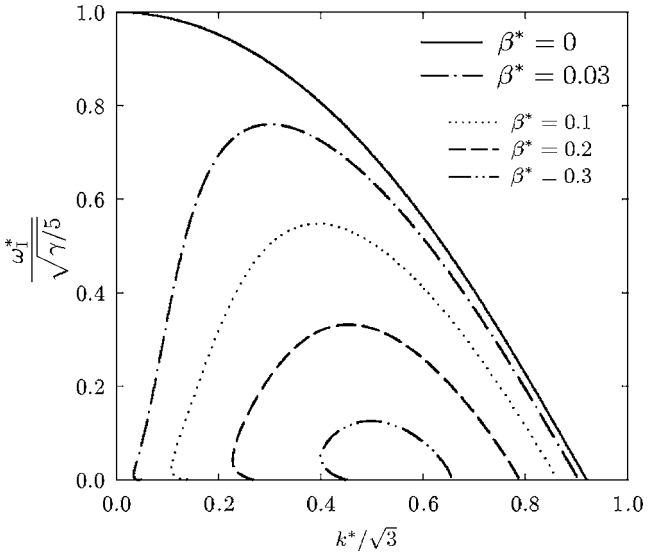

FIG. 1. Growth rate (imaginary part ω_I^* of the complex frequency) as a function of wave number for a horizontal wave ($\hat{\boldsymbol{k}}\cdot\hat{\boldsymbol{z}}=0$), and for a dimensionless center-of-mass diffusivity of $D_\perp^*=0.02$. The various curves correspond to different levels of stratification. The growth rates were computed by numerical solution of the dispersion relation (18) using a bisection algorithm.

The effects of stratification and center-of-mass dispersion on the stability are illustrated in more detail in Fig. 2, showing the range of unstable wave numbers as a function of β^* and $D_\perp^*$. Figure 2(a) confirms the stabilizing effect of stratification; as β^* increases the range of unstable wave numbers shrinks. Beyond $\beta^*\approx 0.32$ all wave numbers become stable, where this value of β^* depends on the value chosen for the dispersion coefficient $D_\perp^*$. In addition, a stronger center-of-mass dispersion is also shown to reduce the range of unstable wave numbers [Fig. 2(b)]. Dispersion how-

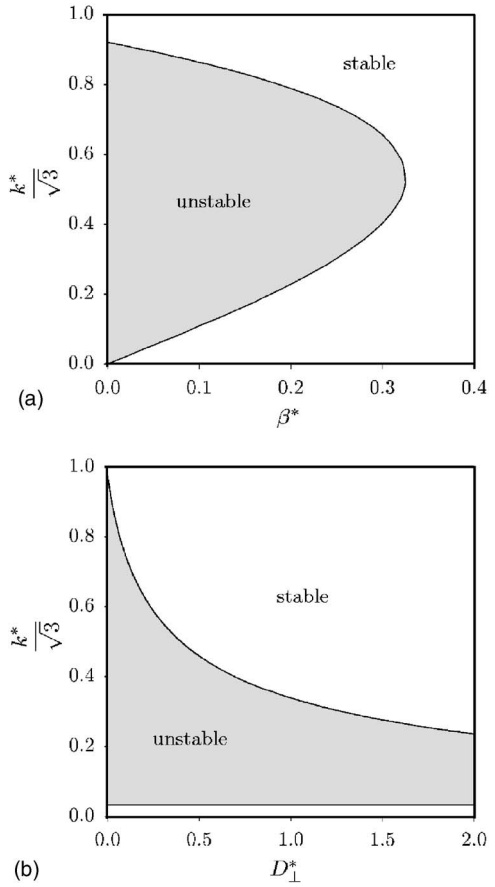

FIG. 2. Range of unstable wave numbers as a function of (a) the stratification parameter β^* (for a constant dispersion coefficient of $D_\perp^*=0.02$), and of (b) the dispersion coefficient $D_\perp^*$ (for a stratification parameter of $\beta^*=0.03$).

ever predominantly affects high wave numbers, and is less efficient than stratification at suppressing the instability.

Additional insight can be gained into the respective leading-order effects of stratification and dispersion by seeking perturbation solutions in the limit of long waves ($k^* \ll 1$). When stratification is present ($\beta^* > 0$), the leading terms in an expansion of the dispersion relation (18) for small $|\boldsymbol{k}^*|$ are found to be

$$\omega^* + i\frac{\beta^*}{k^{*2}} + O(1/k^*) = 0, \tag{19}$$

hence the growth rate, $\omega_I^* = -\beta^*/k^{*2} + O(1/k^*)$. The main effect of stratification is therefore to damp the fluctuations at low wave numbers (or long wavelengths), in agreement with the numerical solution shown in Fig. 1.

On the other hand, in the absence of stratification ($\beta^*=0$), we find that expanding Eq. (18) in the limit of small $|\boldsymbol{k}^*|$ yields the following algebraic equation:

$$\omega^{*4} + \frac{\gamma}{5}\omega^{*2} - i\frac{2\gamma D_\perp^*}{5}k^{*2}\omega^* + \frac{\gamma}{35}k^{*2} + O(k^{*3}) = 0. \tag{20}$$

A solution of Eq. (20) is obtained as a perturbation expansion, $\omega^* = \omega_0 + \omega_1 k^* + \omega_2 k^{*2} + O(k^{*3})$. After manipulation, the growth rate or imaginary part of the complex frequency is found as

$$\omega_I^* = \pm\left(\frac{\gamma}{5}\right)^{1/2} - k^{*2}\left[D_\perp^* \pm \frac{1}{70}\left(\frac{5}{\gamma}\right)^{3/2}\right] + O(k^{*3}). \tag{21}$$

The leading-order effect of center-of-mass dispersion on the concentration fluctuations is to damp the growth rate at high wave numbers as $-k^{*2}D_\perp^*$. This effect is similar to that described in our previous work[14] in the case of sedimenting deformable particles. However, center-of-mass dispersion is not the only mechanism resulting in damping at high wave numbers; even in the absence of dispersion, ω_I^* decays with k^* in agreement with the original stability analysis of Koch and Shaqfeh.[6] One should also note that the two scalings for the leading-order effects of stratification ($\omega_I^* \sim -\beta^*/k^{*2}$) and of diffusion ($\omega_I^* \sim -D_\perp^* k^{*2}$), which were obtained here in the limit of $k^* \ll 1$, are in fact valid for arbitrary k^* as can easily be shown from the linearized conservation equation (15). This will justify the use of these expressions in Sec. III when deriving a scaling for the most unstable mode in a stratified suspension.

E. Anisotropic case

Experiments[8] and numerical simulations[10–15] both show that sedimenting rods tend to align in the direction of gravity as a result of the vertical shear between the dense clusters and clarified regions. It is therefore useful to investigate how the instability is modified when the orientation distribution is anisotropic. Here, we limit ourselves to distributions that are axisymmetric with respect to the direction of gravity, i.e., $\Psi(\boldsymbol{p}) = \Psi(\alpha)$, where $\alpha = \boldsymbol{p}\cdot\hat{\boldsymbol{z}}$. In that particular case, the gradient of Ψ appearing in the dispersion relation becomes

$$\nabla_p \Psi(\boldsymbol{p}) = \frac{d\Psi}{d\alpha}(\mathbf{I} - \boldsymbol{pp})\cdot\hat{\boldsymbol{z}}, \tag{22}$$

which greatly simplifies the evaluation of the second integral in Eq. (17). The dispersion relation (17) was solved numerically for an Onsager orientation distribution,[24] in which the degree of anisotropy is parameterized by a scalar m:

$$\Psi(\alpha) = \frac{m\cosh(m\alpha)}{4\pi\sinh(m)}. \tag{23}$$

The isotropic distribution is recovered when $m=0$, while $m \to \infty$ corresponds to a fully aligned suspension. The solutions for the growth rates of horizontal waves for various values of m are shown in Fig. 3. In Fig. 3(a), both stratification and diffusion are neglected ($\beta^*=0$, $D_\perp^*=0$), which allows us to isolate the effects of anisotropy. In particular, we observe that anisotropy tends to reduce the growth rates at all wavelengths. This stabilizing effect is easily understood; vertically aligned rods have very weak horizontal velocities, which hinders their lateral migration and thereby reduces their ability to form clusters. Note that in very anisotropic suspensions ($m \geq 4.75$ approximately), the longest modes are no longer the most unstable, and a maximum growth rate appears at a finite wave number. This suggests that anisotropy could in principle result in a wave number selection; no such effect was however observed in simulations, where the orientation distribution quickly adjusts to the flow conditions. When both stratification and diffusion are present [Fig.

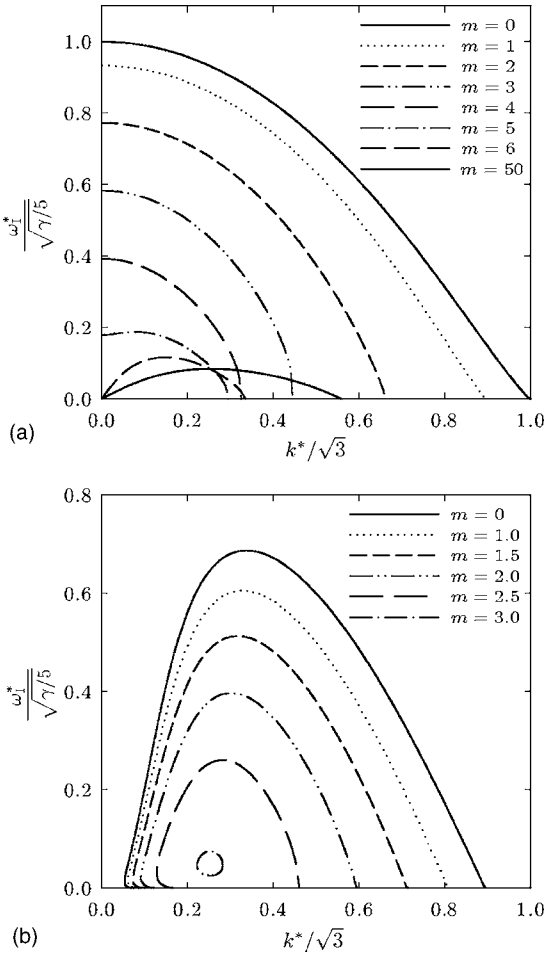

FIG. 3. Growth rate (imaginary part ω_I^* of the complex frequency) as a function of wave number for a horizontal wave ($\hat{\boldsymbol{k}}\cdot\hat{\boldsymbol{z}}=0$) in anisotropic suspensions. The various curves correspond to different degrees of anisotropy, parameterized by the coefficient m in the Onsager distribution equation (23). The growth rates were computed by numerical solution of the dispersion relation (17) using a bisection algorithm. In plot (a) stratification and diffusion are neglected ($\beta^*=0, D_\perp^*=0$); in plot (b) they are set to $\beta^*=0.05$, $D_\perp^*=0.02$.

3(b)], a wave number selection is expected for all values of m for the reasons discussed in Sec. II D, and the effect of particle alignment is to reduce the growth rates at all wave numbers.

The largest unstable wave number in the absence of stratification and of diffusion can be obtained analytically by setting $\omega^*\equiv 0$ in Eq. (17) and solving for k^*. The result is found to be

$$k_{\max}^* = \left[3\gamma + \int\left(\gamma\alpha + \frac{\gamma+1}{2\alpha}\right)\frac{d\Psi}{d\alpha}d\boldsymbol{p}\right]^{1/2}, \tag{24}$$

and the range $[0, k_{\max}^*]$ of unstable wave numbers is shown in Fig. 4 for Onsager distributions as a function of the parameter m. As expected from Fig. 3, the effect of anisotropy is to shrink the range of unstable wave numbers. Note however that the range is not reduced monotonically; the initial decay is followed by a small increase and a saturation, also visible in Fig. 3(a). In very anisotropic suspensions there always remains a finite range of unstable modes; the corresponding growth rates however keep decreasing with m, and in the limit of perfect alignment ($m=\infty$) the suspension is neutrally stable.

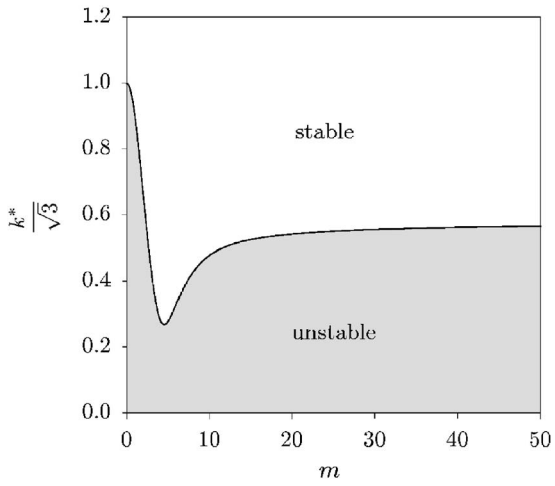

FIG. 4. Range of unstable wave numbers for a horizontal wave in an anisotropic suspension as a function of the Onsager parameter m [Eq. (23)]. Both stratification and diffusion are neglected ($\beta^*=0$, $D_\perp^*=0$).

As previously done in the isotropic case (Sec. II D), we can also obtain the behavior at low wave numbers by seeking a perturbation solution to the dispersion relation. When stratification is included ($\beta^*>0$), the result of Eq. (19) remains unchanged to the order retained in the expansion:

$$\omega_I^* = -\frac{\beta^*}{k^{*2}}\int\Psi(\alpha)d\boldsymbol{p} + O(1/k^*) = -\frac{\beta^*}{k^{*2}} + O(1/k^*). \tag{25}$$

The effects of anisotropy become clearer in the absence of stratification ($\beta^*=0$). An expansion of Eq. (17) for a horizontal wave in the limit of $|\boldsymbol{k}^*|\ll 1$ indeed yields the following algebraic equation:

$$\omega^{*4} + a(\Psi)\omega^{*2} - 2iD_\perp^* a(\Psi)k^{*2}\omega^* + b(\Psi)k^{*2} + O(k^{*3}) = 0, \tag{26}$$

which is very similar to Eq. (20) for the isotropic case, but where the coefficients $a(\Psi)$ and $b(\Psi)$ now depend on the orientation distribution. More precisely, a and b can be expressed in terms of moments of the orientation vector $\boldsymbol{p}$. Introducing the following notations:

$$\mathbf{M}_i = \int\Psi(\alpha)\underbrace{\boldsymbol{p}\ldots\boldsymbol{p}}_{i\text{ times}}d\boldsymbol{p}, \quad \mathbf{N}_i = \int\frac{d\Psi}{d\alpha}\underbrace{\boldsymbol{p}\ldots\boldsymbol{p}}_{i\text{ times}}d\boldsymbol{p}, \tag{27}$$

and

$$\hat{\boldsymbol{k}}^{(i)}\hat{\boldsymbol{z}}^{(j)} = \underbrace{\hat{\boldsymbol{k}}\ldots\hat{\boldsymbol{k}}}_{i\text{ times}}\underbrace{\hat{\boldsymbol{z}}\ldots\hat{\boldsymbol{z}}}_{j\text{ times}}. \tag{28}$$

The scalar coefficients a and b are found as

$$a(\Psi) = 3\gamma\mathbf{M}_4:(\hat{\boldsymbol{k}}^{(2)}\hat{\boldsymbol{z}}^{(2)}) - \frac{\gamma+1}{2}\mathbf{N}_3:(\hat{\boldsymbol{k}}^{(2)}\hat{\boldsymbol{z}}) + \gamma\mathbf{N}_5:(\hat{\boldsymbol{k}}^{(2)}\hat{\boldsymbol{z}}^{(3)}), \tag{29}$$

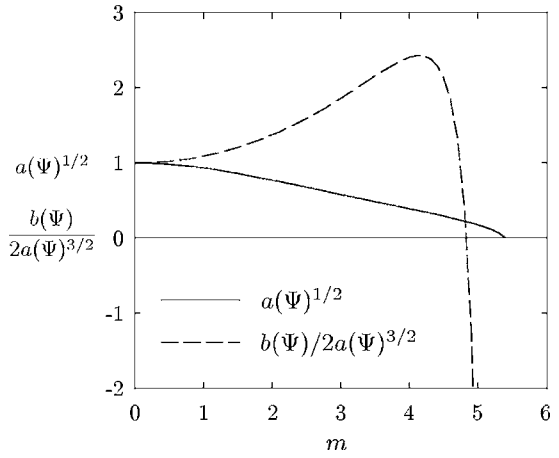

FIG. 5. Coefficients $a(\Psi)^{1/2}$ and $b(\Psi)/2a(\Psi)^{3/2}$ in the long-wave expansion equation (31) for an Onsager orientation distribution [Eq. (23)] as a function of the parameter m. Both coefficients are normalized by their value at $m=0$ (isotropic limit).

$$b(\Psi) = 3\gamma \mathbf{M}_8 : (\hat{\boldsymbol{k}}^{(4)}\hat{\boldsymbol{z}}^{(4)}) - \frac{\gamma+1}{2}\mathbf{N}_7 : (\hat{\boldsymbol{k}}^{(4)}\hat{\boldsymbol{z}}^{(3)}) + \gamma \mathbf{N}_9 : (\hat{\boldsymbol{k}}^{(4)}\hat{\boldsymbol{z}}^{(5)}), \tag{30}$$

where the symbol : denotes the scalar product between the tensors on each side.

The solution of Eq. (26) for $k^* \ll 1$ can be shown to be pure imaginary with imaginary part:

$$\omega_I^* = \pm a(\Psi)^{1/2} - k^{*2}\left[D_\perp^* \pm \frac{b(\Psi)}{2a(\Psi)^{3/2}}\right] + O(k^{*3}). \tag{31}$$

This solution is similar to Eq. (21) for the isotropic case. In particular, an interesting observation is that the leading order effect of diffusion is unaffected by the orientation distribution. The two coefficients $a(\Psi)^{1/2}$ and $b(\Psi)/2a(\Psi)^{3/2}$ now depend on the orientation distribution as expected from Fig. 3, and are plotted in Fig. 5 for the Onsager distribution of Eq. (23) as a function of m. As expected from Fig. 3, $a(\Psi)^{1/2}$ decreases as m increases and becomes zero for $m \geq 5.5$ approximately, confirming that a strongly aligned suspension is stable at zero-wave number. The second derivative of $\omega^*(k^*)$ at $k^*=0$, which is related to $b(\Psi)/2a(\Psi)^{3/2}$, is also observed to change sign at a finite value of m, in agreement with the observations made earlier in Fig. 3.

III. SCALING ANALYSIS

The analysis of the previous section showed that the growth of concentration fluctuations can be damped at low wave numbers by stratification and at high wave numbers by center-of-mass dispersion. The wave number for the most unstable mode in a stratified suspension can therefore be determined by balancing these two effects [Eqs. (19) and (21)]:

$$-\frac{\beta^*}{k^{*2}} \sim -k^{*2}\left[D_\perp^* + \frac{1}{70}\left(\frac{5}{\gamma}\right)^{3/2}\right]. \tag{32}$$

The hydrodynamic diffusivity $D_\perp^*$ models the randomizing effect of velocity fluctuations arising in the suspension over long times, and is expected to be a function of the suspension structure and concentration. Its scaling with the wave number k^* and with the volume fraction ϕ must therefore be determined. Since the velocity fluctuations which result in hydrodynamic dispersion are driven by concentration fluctuations occurring over length scales of the order of k^{-1}, we expect the dimensional diffusivity to scale as $D_\perp \sim \Delta U k^{-1}$, where ΔU is the magnitude of the velocity fluctuations. In turn, ΔU is determined by balancing the gravity force and the Stokes drag acting on a typical concentration fluctuation of size k^{-1}: $\Delta N V_p \Delta\rho g \sim \mu k^{-1}\Delta U$, where ΔN is the excess number of particles in the concentration fluctuation.[1,2] Since concentration fluctuations in the suspension grow as a result of the instability, their magnitude ΔN evolves in time and is unknown *a priori*. Let us consider the onset of the instability in a random suspension, which is described by Poisson statistics: $\Delta N \sim (\phi k^{-3}/V_p)^{1/2}$. This assumption, whose validity will have to be assessed, results in the following scaling for the magnitude of the velocity fluctuations and for the diffusivity: $\Delta U \sim U_0 (kl)^{-1/2}\phi^{1/2}$, and $D_\perp \sim U_0 l (kl)^{-3/2}\phi^{1/2}$, where $U_0 = \Delta\rho V_p g/\mu l$ is the scale for the sedimentation velocity of an isolated particle of length l.

This scaling for the hydrodynamic diffusivity can be substituted into Eq. (32). When center-of-mass diffusion is the dominant mechanism for damping at high wave numbers $(D_\perp^* \gg (5/\gamma)^{3/2}/70)$, we obtain the following scaling for the most unstable wave number:

$$kl \sim (\beta l)^{2/5}\phi^{1/5}. \tag{33}$$

On the other hand, if center-of-mass diffusion is negligible $(D_\perp^* \ll (5/\gamma)^{3/2}/70)$, a different scaling is expected:

$$kl \sim (\beta l)^{1/4}\phi^{3/8}. \tag{34}$$

Equivalently, the characteristic size of the density fluctuations in the suspension will be given by $\xi = k^{-1}$. Note that in both Eq. (33) and Eq. (34) the proportionality constant may depend on the particle aspect ratio. These predictions will be tested against simulation data in Sec. IV B, where we will see that good agreement with Eq. (33) is observed, suggesting that hydrodynamic dispersion is in practice the main mechanism for the damping of high-wave number fluctuations.

Interestingly, the first scaling for ξ [Eq. (33)] is the same as that found by Mucha *et al.*[5,17] for the correlation length in a stratified suspension of sedimenting spheres. In that particular case, the physical mechanism that they proposed goes as follows. As in the previous discussion, a concentration fluctuation of characteristic size ξ, which has a magnitude of $\Delta\phi \sim (\phi l^3/\xi^3)^{1/2}$ for Poisson statistics, creates a velocity fluctuation of scale $\Delta U \sim U_0(\xi/l)^{1/2}\phi^{1/2}$ as it sediments. This velocity fluctuation, however, only occurs if there is a true density mismatch with the surrounding fluid, i.e., if the size of the concentration fluctuation remains below the length scale over which stratification changes the background volume fraction ϕ by $\Delta\phi$. This length scale is given by $\Delta\phi/(\beta\phi)$. The maximum value for the correlation length therefore satisfies $\xi \sim (\phi l^3/\xi^3)^{1/2}/(\beta\phi)$, from which the scaling of Eq. (33) is easily obtained.

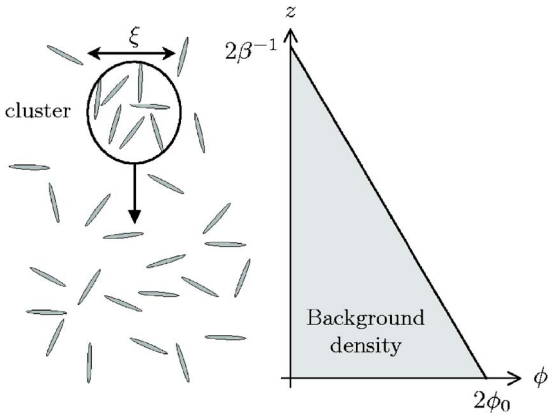

FIG. 6. Schematic illustrating the effect of stratification on the growth of density fluctuations: a cluster containing a concentration fluctuation of size $\Delta\phi$ only grows if its extent ξ is less than the height $\Delta\phi/\beta\phi$ over which the background concentration changes by $\Delta\phi$ as result of stratification.

As illustrated in Fig. 6, a qualitatively similar mechanism can be expected in the case of sedimenting spheroids. A cluster of particles, which has a certain density mismatch with the surrounding fluid, can only travel a certain distance in a stably stratified suspension until the mismatch becomes negligible. The fact that the scaling we obtained in Eq. (33) is the same as for sedimenting spheres is a direct consequence of the assumption made above of Poisson statistics over the length scale of the fluctuations. This assumption is justified at the onset of the instability when the arrangement of the particles is random, and suggests that initially at least the growth of the concentration fluctuations is directly governed by the velocity fluctuations. At later times however, the statistics clearly will depart from Poisson owing to the clustering of the particles; the validity of Eq. (33) may then become questionable, and will need to be tested against simulations.

IV. NUMERICAL SIMULATIONS

A. Simulation method

We use the simulation method of Saintillan *et al.*,[14] which is only outlined here. The method consists of tracking the position $\boldsymbol{x}_\alpha$ and orientation $\boldsymbol{p}_\alpha$ of a given spheroid $\alpha=1,\ldots,N$ in the suspension using the following dynamic equations:

$$\dot{\boldsymbol{x}}_\alpha = \boldsymbol{U}_s(\boldsymbol{p}_\alpha) + \boldsymbol{u}(\boldsymbol{x}_\alpha), \tag{35}$$

$$\dot{\boldsymbol{p}}_\alpha = (\mathbf{I} - \boldsymbol{p}_\alpha\boldsymbol{p}_\alpha)\cdot[\gamma\mathbf{E}(\boldsymbol{x}_\alpha) + \boldsymbol{\Omega}(\boldsymbol{x}_\alpha)]\cdot\boldsymbol{p}_\alpha, \tag{36}$$

which are similar to Eqs. (2) and (5). Hydrodynamic interactions are captured through the disturbance velocity $\boldsymbol{u}$ (and the corresponding rate of strain and rate of rotation tensors, $\mathbf{E}$ and $\boldsymbol{\Omega}$), which satisfies the Stokes equations:

$$-\mu\nabla^2\boldsymbol{u} + \nabla p = \boldsymbol{f}(\boldsymbol{x}), \quad \nabla\cdot\boldsymbol{u} = 0. \tag{37}$$

The body force field $\boldsymbol{f}(\boldsymbol{x})$ captures the effects of the particles on the fluid, and to leading order corresponds to a point force applied at the center of each spheroid. Instead of using actual point singularities, we use a Cartesian grid and assign the forces exerted by the particles on the fluid to the neighboring mesh points $\boldsymbol{x}_i$:

$$\boldsymbol{f}(\boldsymbol{x}_i) = \sum_{\alpha=1}^{N} \boldsymbol{F}M(\boldsymbol{x}_i - \boldsymbol{x}_\alpha), \tag{38}$$

where $M(\boldsymbol{x})$ is a smooth assignment function, which is chosen to satisfy certain properties.[14] In this work third-order B-splines are used.[25] Finally, the Stokes equations (37) are solved numerically using an expansion of the velocity as a sum of Fourier modes satisfying a tangential flow boundary condition on the container boundaries;[4,14] while this differs from the exact no-slip boundary condition for viscous flow, the absence of fluid penetration at the bottom of the container was previously shown to qualitatively capture the effects of container walls. In particular, we observed in our previous work that such a boundary condition is sufficient to capture a wave number selection in sedimenting suspensions of spheroids.[14] In the remainder of the paper distances are made dimensionless with the length $l_c=l$ of the major axis of the particles, velocities with the sedimentation speed $u_c=(\lambda_0+\lambda_1)\Delta\rho V_p g$ of a vertical spheroid at infinite dilution, and times with the time $t_c=l_c/u_c$ for a vertical spheroid to sediment over the length of its major axis.

B. Fluctuations in stably stratified suspensions

We first test the conclusions of the stability analysis of Sec. II by performing simulations of suspensions in which a vertical density gradient is imposed in the initial configuration. As a measure of the characteristic size of the structures that develop in the suspension, we use the correlation length ξ defined as the position of the first minimum in the autocorrelation function $C_{zz}(x)$ of the vertical fluid velocity component in the horizontal direction:

$$C_{zz}(x) = \int u_z(x')u_z(x'+x)dx'. \tag{39}$$

In our previous work[14] we showed indeed that the velocity field decorrelates in the horizontal direction over a distance of the order of the size of the clusters in the suspension, since these entrain the fluid with them and are surrounded by backflow regions. This measure has also been used successfully in experiments to estimate the size of the clusters in fiber suspensions.[9] To isolate the effects of the initial stratification, ξ is measured at time $t=15$ shortly after the start of the simulations, which corresponds approximately to the occurrence of the peak in the velocity fluctuations;[14] this time is short enough for the stratification to remain roughly constant, but sufficiently long for the inhomogeneities to start forming in the suspension.

Typical velocity autocorrelation functions in nonstratified and stratified suspensions are shown in Fig. 7(a). In the absence of stratification ($\beta=0$), the velocity field decorrelates over half a box width ($\xi=L_x/2$), indicating the formation of a single streamer spanning the full width of the box. This agrees qualitatively with experimental observations[9] and our previous simulations[14] in homogeneous suspensions shortly after the start of sedimentation, and is also predicted

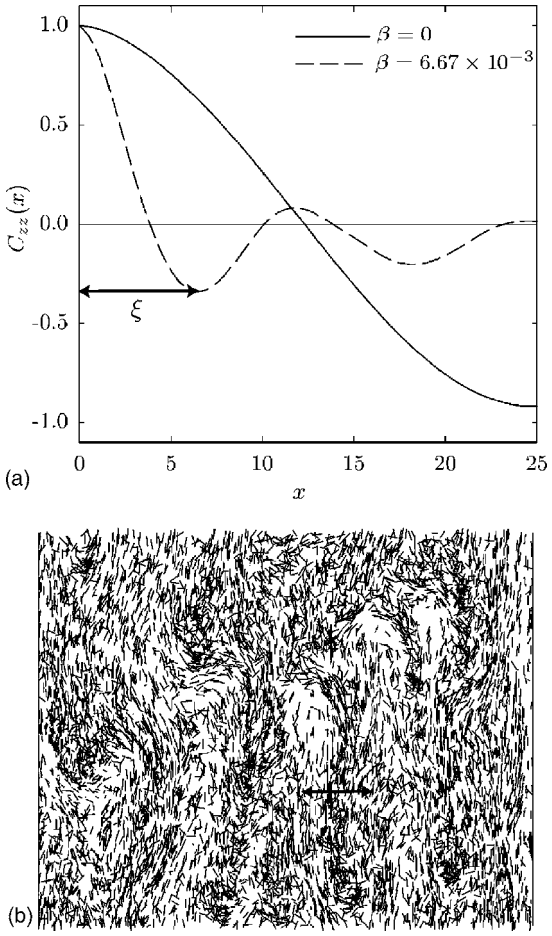

FIG. 7. (a) Autocorrelation function $C_{zz}(x)$ in the horizontal direction of the vertical disturbance fluid velocity, in a suspension of 257 831 spheroids of aspect ratio $A=15$ in a box of dimensions $L_x=50$, $L_y=20$, $L_z=300$ (volume fraction $\phi=0.2\%$), measured at $t=15$ near the peak of the fluctuations, with and without stratification. The correlation length ξ is measured as the position of the first minimum. (b) Visualization of the suspension of (a) at $t=15$ in the stratified case ($\beta=6.67\times10^{-3}$), where a wave number selection is observed. The arrow represents the correlation length measured in (a).

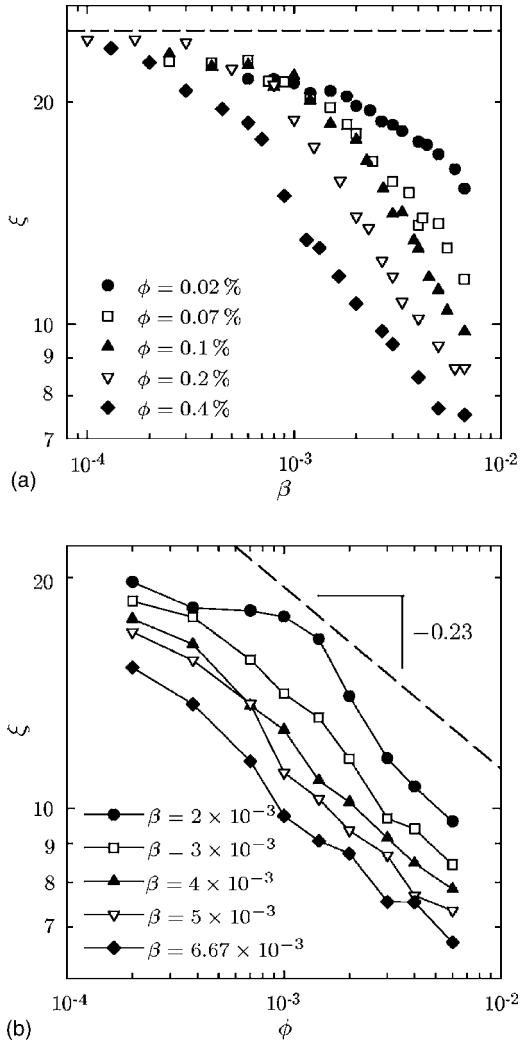

FIG. 8. Correlation length ξ in the horizontal direction, measured as the first minimum in the autocorrelation function of the vertical fluid velocity component (see Fig. 7), as a function of (a) the stratification parameter β in the suspension, and (b) the local volume fraction ϕ. The stratification was imposed in the initial particle distributions, and the correlation length was measured at $t=15$ near the center of the box. The simulations were run in a box of dimensions $L_x=50$, $L_y=20$, $L_z=300$, and are for spheroids of aspect ratio $A=15$. Each point on the graphs is an average over 20–30 simulations. The dependence of ξ on the volume fraction ϕ is well approximated by a power law with exponent ≈-0.23.

by the original stability analysis of Koch and Shaqfeh[6] for a homogeneous base state, in which the longest wavelength dominates. The behavior is quite different, however, when stratification is imposed. When $\beta=6.67\times10^{-3}$ in Fig. 7(a), the correlation length is found to be much shorter, of the order of a few particle lengths. Figure 7(b) shows the corresponding particle distribution, on which the correlation length ξ is denoted by an arrow; the particle distribution indeed presents several distinct clusters in the lateral direction, the characteristic size of which is of the order of ξ. These observations confirm the stabilizing influence of stratification and its role in selecting the size or wavelength of the inhomogeneities in the suspension.

The effects of the density gradient β on the wavelength of the instability are shown more quantitatively in Fig. 8(a), where the correlation length ξ is plotted vs β for various volume fractions ϕ. In very weakly stratified suspensions ($\beta\sim10^{-4}$), the correlation length saturates at approximately half a box width, showing that the wavelength is selected by the size of the container. When β increases, ξ is found to decrease, yielding cluster sizes that are controlled by stratification and do not depend on the container dimensions. At a given value of β, the correlation length is observed to be larger in more dilute suspensions.

The dependence on concentration is shown more precisely in Fig. 8(b), where ξ is shown as a function of ϕ for a few given values of β. The correlation length indeed decreases with increasing volume fraction, and the decay is well described by the following power law: $\xi\sim\phi^{-0.23}$. The data of Fig. 8(a) rescaled with $\phi^{-0.23}$ are shown in Fig. 9, where the curves corresponding to various volume fractions are observed to collapse onto a single straight line in a log-log plot, with departures at small values of β owing to box-size effects. We therefore find the following scaling for the correlation length when box-size effects are negligible (i.e., when $\xi<L_x/2$):

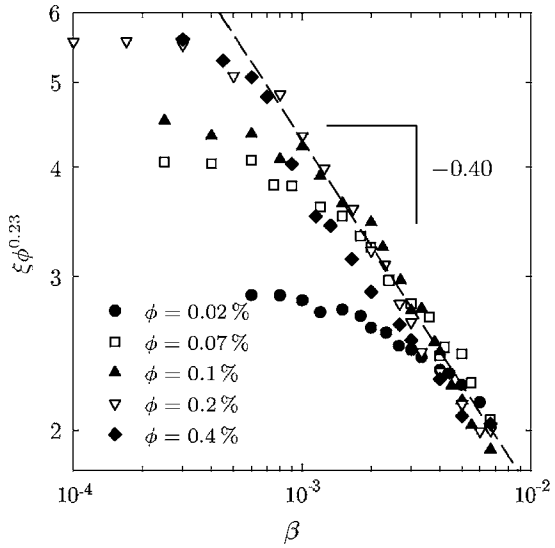

FIG. 9. Correlation length ξ in the horizontal direction, scaled by $\phi^{-0.23}$, as a function of the stratification parameter β at various volume fractions. The data are the same as in Fig. 8(a). At high values of β the curves asymptote to a power law with exponent ≈ -0.40.

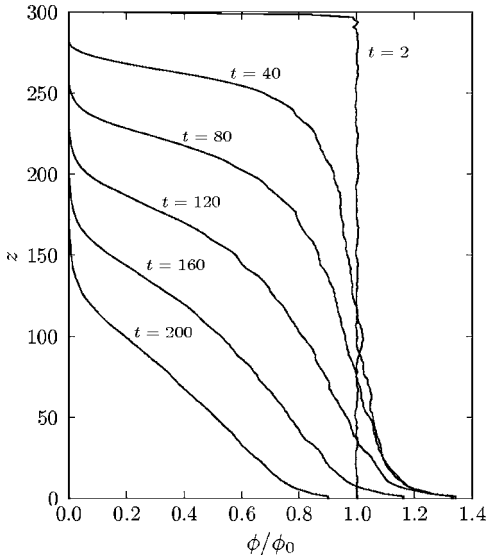

FIG. 10. Evolution of the vertical concentration profile with time in a suspension of 257 831 spheroids of aspect ratio $A=15$ in a box of dimensions $L_x=50$, $L_y=20$, $L_z=300$ (volume fraction $\phi_0=0.2\%$). Each curve shows an average over 20 simulations. The local volume fraction ϕ is normalized by the bulk value ϕ_0 at $t=0$.

$$\xi \approx C\beta^{-0.40}\phi^{-0.23}, \tag{40}$$

where the dimensionless constant C is of the order of 0.3.

The exponents found in Eq. (40) are in good agreement with the theoretical prediction of Eq. (33), but do not agree with the other proposed scaling [Eq. (34)]; this suggests as explained in Sec. III that the center-of-mass dispersion is the main mechanism for damping at high wave numbers. Small departures are expected to occur for a variety of reasons. Most importantly, the theoretical scaling was derived based on the assumption that the particle distribution on the length scale of the fluctuations can be described by Poisson statistics. While this is strictly true at $t=0$, the distribution then evolves as a result of the instability, leading to stronger density fluctuations and a possibly different scaling for the hydrodynamic diffusivity. The good agreement between simulations and theory suggests that these effects are weak, at least initially. Finite-box effects are also likely to influence the results from the simulations, in particular in the more dilute cases or when the stratification is very weak; this is, for instance, clear at the low volume fraction of $\phi=0.02\%$ in Figs. 7(a) and 8, where the exponent of -0.40 for the dependence on β is never fully reached.

C. Wave number selection process

In initially well-mixed suspensions, the stratification at $t=0$ is negligible. The onset of the instability is therefore governed by the analysis of Koch and Shaqfeh,[6] and characterized by the formation of a large-scale streamer spanning the width of the container.[9,14] Stratification however is known to develop,[14] and may subsequently have an effect on the wavelength of the instability. The evolution of the vertical concentration profile in a typical simulation is shown in Fig. 10. At $t=0$, the concentration is uniform, but a significant gradient in the vertical direction is observed to appear as the sedimentation progresses. First, the interface between the bulk of the suspension and the clear fluid spreads in time, resulting in the formation of a broad suspension front. This phenomenon can be attributed in part to the difference in the sedimentation rates of spheroids with different orientations. In addition, the bulk of the suspension also becomes stratified, with particles accumulating near the bottom of the container. While the precise mechanism for this effect deserves further consideration, it is likely to be due to the formation of clusters in the suspension, which settle at a higher speed than particles in the clarified regions. At later times, the concentration gradients in the suspension front and in the bulk become comparable, resulting in an almost linear concentration profile in the vertical direction.

The concentration fluctuations are described more quantitatively in Fig. 11, which shows the evolution of the stratification parameter β and of the local volume fraction ϕ at a given vertical station during the sedimentation. Figure 11(a) confirms that the stratification, which is initially negligible ($\beta \approx 0$), becomes significant with values of β reaching 0.03 at $t=200$. Note that such gradients are much stronger than those investigated in Sec. IV B, where the largest value for β did not exceed 0.01; significant effects on the wavelength of the instability can therefore be anticipated. The local concentration at a given height in the container also decreases in time, as shown in Fig. 11(b). In particular, the simulations show that the decay begins quite early (before the approach of the sedimentation front), and is therefore at first a consequence of the stratification in the bulk. Note however that very near the bottom of the container the concentration first increases, as can be seen in Fig. 10.

Figure 12(a) illustrates the wave number selection process of the concentration instability. The correlation length ξ in the horizontal direction during sedimentation, measured at the same height in the container as β and ϕ in Fig. 11, is plotted vs time. The trends observed agree with previous

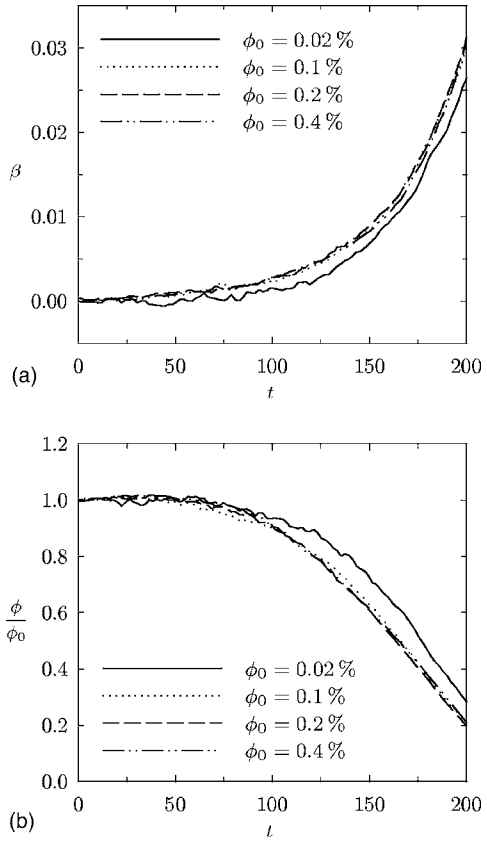

FIG. 11. Time evolution of (a) the stratification parameter β, and (b) the normalized volume fraction ϕ/ϕ_0, over the course of a simulation. The simulations are for spheroids of aspect ratio $A=15$ and were performed in a box of dimensions $L_x=50$, $L_y=20$, $L_z=300$. Both β and ϕ/ϕ_0 were measured at a height of $z=100$ in the container. The curves are averaged over 20 simulations.

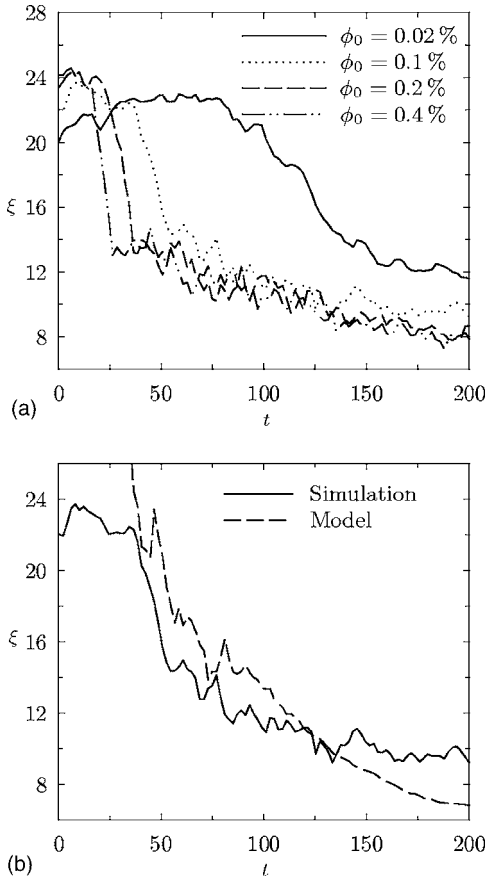

FIG. 12. (a) Time evolution of the correlation length ξ in the horizontal direction. The simulations are for spheroids of aspect ratio $A=15$ and were performed in a box of dimensions $L_x=50$, $L_y=20$, $L_z=300$. The correlation length was measured at a height of $z=100$ in the container. The curves are averaged over 20 simulations. (b) Comparison between the correlation length measured in the simulations (in the case $\phi_0=0.1\%$), and the prediction of Eq. (40), in which the data of Fig. 11 were used for the local evolution of β and ϕ.

observations;[9,14] initially the correlation length is of the order of the box width ($\xi \approx L_x/2$), after which it undergoes a transition to a much shorter value of the order of a few particle lengths ($\xi \approx 8$ to 12 in Fig. 12). While Fig. 12(a) suggests a saturation at long times, no true steady state is observed and ξ continues to decay until the end of settling. The very slow decay of ξ, however, may explain why the microstructure in our previous simulations on smaller systems appeared to reach a steady state.[14] The influence of concentration is also shown in Fig. 12, where we see that the transition from a single streamer to multiple clusters occurs more rapidly in the concentrated suspensions, where the final correlation length is also typically shorter. The effects of concentration are nonetheless quite weak, except in the most dilute case ($\phi_0=0.02\%$), where the transition to small-scale structures occurs at a significantly later time.

To quantitatively assess the role played by stratification in the evolution of the correlation length shown in Fig. 12(a), we compare in Fig. 12(b) the measured correlation length to that predicted by the scaling of Eq. (40), in which we use the data of Fig. 11 for the evolution of the stratification parameter β and of the local volume fraction ϕ. While the model does not reproduce the saturation at half a box width at short times, which is a finite-box effect, it does capture the subsequent time decay of the correlation length. The predicted decay is slightly faster than observed in the simulations, yet the measured and predicted correlation lengths never differ by more than approximately 20%. This agreement is surprisingly good in light of the approximations made in Sec. III when deriving the scaling, and strongly suggests that the wave number selection is controlled by stratification at least in these simulations. An important remark is that the initial decay of ξ occurs quite early in Fig. 12(b) (between $t=50$ and 75 for both the measured and predicted curves), at a time when the stratification in the suspension is still very weak as seen in Fig. 11(a) ($\beta \approx 2\times 10^{-3}$); this demonstrates that relatively weak density gradients can have sizable effects on the wave number selection of the instability. Note that a similar remark had been made by Mucha *et al.* regarding the effect of stratification on the correlation length in sphere suspensions.[5]

The theoretical scaling for the correlation length also allows us to understand several of the features observed in Fig. 12(a). In particular, since the stratification parameter β is sensibly the same at all volume fractions [Fig. 11(a)], the main effect of volume fraction on the wave number selection occurs through the scaling with ϕ in Eq. (40); we can there-

fore expect the correlation length to be larger in more dilute suspensions, and hence the transition from a box-dependent streamer to multiple clusters to occur at a later time, as indeed observed in the simulation data. The saturation of ξ near the end of the sedimentation process can also be explained. Whereas the vertical density gradient (or stratification parameter β) keeps increasing in time [Fig. 11(a)], the local volume fraction, which is initially constant, drops considerably as the front approaches [Fig. 11(b)]; the competing effects of increasing stratification and decreasing volume fraction may therefore be responsible for the saturation of ξ, according to Eq. (40).

V. CONCLUDING REMARKS

We have used theory and numerical simulations to investigate the effects of stratification on the concentration instability that occurs in suspensions of spheroidal particles under sedimentation. First we performed a linear stability analysis in a stably stratified suspension, and showed that stratification provides a mechanism for damping of the fluctuations at low wave numbers, while high-wave-number fluctuations are suppressed by hydrodynamic dispersion. The balance of these two effects therefore results in a selection of a most unstable mode at a finite wave number. Based on the results of the stability analysis, we were able to derive the following scaling for the characteristic size of the fluctuations: $\xi/l \sim (\beta l)^{-2/5}\phi^{-1/5}$. This scaling, which is the same as that previously obtained for the size of the fluctuations in sphere suspensions,[5,17] is based on an assumption of Poisson statistics over the length scale of the fluctuations, and is therefore only rigorous at the onset of the instability. Simulations were performed in which a density gradient was imposed at $t=0$, and showed good agreement with the predicted scaling. In initially well-mixed suspensions, we observed that the continuous decay of the wavelength of the fluctuations is also described reasonably well by the same model.

While the present work demonstrates that an accurate description of the concentration instability should take stratification into account, it is by no means proof that the wave number selection in a real system is only governed by the mechanisms described herein. In particular, other effects which have not been accounted for in our analysis are likely to play a role as well. One such effect is hydrodynamic screening by the container side walls, which is a consequence of the no-slip boundary condition on solid boundaries and is not captured by the tangential flow boundary condition used in our simulations. As described previously by Brenner in the case of spheres,[26] no-slip walls provide an additional cutoff for hydrodynamic interactions between the suspended particles, which become negligible beyond distances of the order of the shortest wall separation distance. Other effects may also arise owing to close particle interactions; while our simulations neglected contact and lubrication forces, these may become important inside the clusters, creating entanglements and thereby reinforcing the fluctuations over short distances. In particular, this may result in stronger departures from the Poisson statistics than is the case in our simulations.

One remaining question which was not resolved here is the exact process leading to the formation of the vertical density gradients in the suspension. While the broadening of the front at the top of the suspension can be understood from the differential settling of particles with different orientations, the reason for the formation of gradients in the bulk of the suspension is not entirely clear. Models have been proposed previously to describe stratification in sphere suspensions,[5,27] and were based on solutions of a convective-diffusion equation for the particle phase, in which closure approximations were used for the hydrodynamic diffusivity. One could envisage developing a similar framework in the case of anisotropic particles; yet the presence of clusters in the suspension, which settle at higher rates than the remainder of the particles, would have to be considered. Since the size of these clusters may itself be controlled by stratification, a coupled model for the vertical density profile and for the microstructure may be required.

ACKNOWLEDGMENTS

D.S. is indebted to Michael P. Brenner for a stimulating discussion, and acknowledges funding from a Gerald J. Lieberman Graduate Fellowship.

[1] R. E. Caflisch and J. H. C. Luke, "Variance in the sedimentation speed of a suspension," Phys. Fluids **28**, 759 (1985).
[2] E. J. Hinch, "Sedimentation of small particles," in *Disorder and Mixing*, edited by E. Guyon, J.-P. Nadal, and Y. Pomeau (Kluwer Academic, Dordrecht, 1988).
[3] H. Nicolai, B. Herzhaft, E. J. Hinch, L. Oger, and É. Guazzelli, "Particle velocity fluctuations and hydrodynamic self-diffusion of sedimenting non-Brownian spheres," Phys. Fluids **7**, 12 (1995).
[4] L. Bergougnoux, S. Ghicini, É. Guazzelli, and J. Hinch, "Spreading fronts and fluctuations in sedimentation," Phys. Fluids **15**, 1875 (2003).
[5] P. J. Mucha, S. Y. Tee, D. A. Weitz, B. I. Shraiman, and M. P. Brenner, "A model for velocity fluctuations in sedimentation," J. Fluid Mech. **501**, 71 (2004).
[6] D. L. Koch and E. S. G. Shaqfeh, "The instability of a dispersion of sedimenting spheroids," J. Fluid Mech. **209**, 521 (1989).
[7] B. Herzhaft, É. Guazzelli, M. B. Mackaplow, and E. S. G. Shaqfeh, "Experimental investigation of the sedimentation of a dilute fiber suspension," Phys. Rev. Lett. **77**, 290 (1996).
[8] B. Herzhaft and É. Guazzelli, "Experimental study of the dimentation of dilute and semi-dilute suspensions of fibres," J. Fluid Mech. **384**, 133 (1999).
[9] B. Metzger, É. Guazzelli, and J. E. Butler, "Large-scales streamers in the sedimentation of a dilute fiber suspension," Phys. Rev. Lett. **95**, 164506 (2005).
[10] M. B. Mackaplow and E. S. G. Shaqfeh, "A numerical study of the sedimentation of fibre suspensions," J. Fluid Mech. **376**, 149 (1998).
[11] J. E. Butler and E. S. G. Shaqfeh, "Dynamic simulations of the inhomogeneous sedimentation of rigid fibres," J. Fluid Mech. **468**, 205 (2002).
[12] E. Kuusela, J. M. Lahtinen, and T. Ala-Nissila, "Collective effects in settling of spheroids under steady-state sedimentation," Phys. Rev. Lett. **90**, 094502 (2003).
[13] D. Saintillan, E. Darve, and E. S. G. Shaqfeh, "A smooth particle-mesh Ewald algorithm for Stokes suspension simulations: The sedimentation of fibers," Phys. Fluids **17**, 033301 (2005).
[14] D. Saintillan, E. S. G. Shaqfeh, and E. Darve, "The growth of concentration fluctuations in dilute dispersions of orientable and deformable particles under sedimentation," J. Fluid Mech. **553**, 347 (2006).
[15] A.-K. Tornberg and K. Gustavsson, "A numerical method for simulations of rigid fiber suspensions," J. Comput. Phys. **215**, 172 (2006).
[16] J. H. C. Luke, "Decay of velocity fluctuations in a stably stratified suspension," Phys. Fluids **12**, 1619 (2000).

[17] S.-Y. Tee, P. J. Mucha, L. Cipelletti, S. Manley, M. P. Brenner, P. N. Segrè, and D. A. Weitz, "Nonuniversal velocity fluctuations of sedimenting particles," Phys. Rev. Lett. **89**, 054501 (2002).
[18] N.-Q. Nguyen and A. J. C. Ladd, "Sedimentation of hard-sphere suspensions at low Reynolds number," J. Fluid Mech. **525**, 73 (2005).
[19] M. A. Turney, M. K. Cheung, R. L. Powell, and M. J. McCarthy, "Hindered settling of rod-like particles measured with magnetic resonance imaging," AIChE J. **41**, 251 (1995).
[20] J. Happel and H. Brenner, *Low Reynolds Number Hydrodynamics* (Prentice-Hall, Englewood Cliffs, 1965).
[21] G. B. Jeffery, "The motion of ellipsoidal particles immersed in a viscous fluid," Proc. R. Soc. London, Ser. A **102**, 161 (1922).
[22] H. Hasimoto, "On the periodic fundamental solutions of the Stokes equations and their application to viscous flow past a cubic array of spheres," J. Fluid Mech. **5**, 317 (1959).
[23] P. G. Drazin and W. H. Reid, *Hydrodynamic Stability* (Cambridge University Press, Cambridge, 1981).
[24] L. Onsager, "The effects of shapes on the interaction of colloidal particles," Ann. Phys. **51**, 627 (1949).
[25] I. J. Schoenberg, *Cardinal Spline Interpolation* (SIAM, Philadelphia, 1973).
[26] M. P. Brenner, "Screening mechanisms in sedimentation," Phys. Fluids **11**, 754 (1999).
[27] P. J. Mucha and M. P. Brenner, "Diffusivities and front propagation in sedimentation," Phys. Fluids **15**, 1305 (2003).